

Adiabatic formation of a matched-beam distribution for an alternating-gradient quadrupole lattice

Mikhail A. Dorf, Ronald C. Davidson, Edward A. Startsev, and Hong Qin
Plasma Physics Laboratory, Princeton University, Princeton, New Jersey 08543, USA

(Received 9 October 2009; accepted 13 November 2009; published online 22 December 2009)

The formation of a quasiequilibrium beam distribution matched to an alternating-gradient quadrupole focusing lattice by means of the adiabatic turn-on of the oscillating focusing field is studied numerically using particle-in-cell simulations. Quiescent beam propagation over several hundred lattice periods is demonstrated for a broad range of beam intensities and vacuum phase advances describing the strength of the oscillating focusing field. Properties of the matched-beam distribution are investigated. In particular, self-similar evolution of the beam density profile is observed over a wide range of system parameters. The numerical simulations are performed using the WARP particle-in-cell code. © 2009 American Institute of Physics. [doi:10.1063/1.3271467]

I. INTRODUCTION

The equilibrium and stability properties of an intense charged particle beam propagating through an alternating-gradient quadrupole focusing lattice are of particular importance for a wide range of applications to high energy and nuclear physics, ion-beam-driven high energy density physics and heavy ion fusion, and nuclear waste transmutation.¹⁻⁵ It is therefore important to develop an improved theoretical understanding of intense beam transport. Although the nonlinear effects of the intense self-fields produced by the beam space-charge provide a significant challenge for analytical studies, various analytical models have been developed to describe an equilibrium beam distribution matched to an alternating-gradient quadrupole focusing lattice.^{1,6,7} To validate prospective models it is particularly important to develop numerical techniques allowing for the formation of a quasiequilibrium beam distribution. Furthermore, numerical schemes describing the quiescent loading of a beam distribution into a transport lattice and minimizing the deleterious effects of beam mismatch are of particular importance for detailed numerical studies of various collective processes and instabilities. This paper develops a numerical method for the formation of a quasiequilibrium beam distribution matched to an alternating-gradient quadrupole focusing lattice by means of the adiabatic turn-on of the oscillating focusing field.

The approach of adiabatic turn-on of the oscillating focusing field has been previously investigated by means of nonlinear δF simulations by Stoltz *et al.*⁸ for the case of a periodic focusing solenoidal lattice. In that work the total distribution function F_b of a beam propagating through a periodic focusing solenoidal field with coupling coefficient $\kappa_z(s+S)=\kappa_z(s)$ is divided into a zero-order part (F_b^0) that propagates through the average focusing field $\bar{\kappa}_z=\text{const}$, plus a perturbation (δF_b), which evolves nonlinearly in the zero-order and perturbed field configurations. It was demonstrated that for the case where the oscillatory component of the coupling coefficient, $\delta\kappa_z(s)=\kappa_z(s)-\bar{\kappa}_z$, turns on adiabatically over many periods of the focusing lattice, the amplitude of

the mismatch oscillations reduces by more than one order of magnitude compared to the case where the field oscillation is turned on suddenly. The technique reported in Ref. 8, however, cannot be applied to the case of an alternating-gradient quadrupole system, because the average component of the focusing field vanishes.

In this paper we generalize the method of adiabatic formation of a matched beam distribution to the case of an alternating-gradient quadrupole lattice. In this generalized approach, an equilibrium beam distribution is initially loaded into a uniform focusing channel with the focusing field given by the smooth-focusing approximation, which describes the average effects of the alternating-gradient lattice.^{1,6,7,9} The oscillating quadrupole focusing field is then adiabatically turned on as the amplitude of the uniform field component is adjusted to maintain the average (smooth-focusing) effects of the total focusing field fixed. It is demonstrated that the generalized method allows for quiescent formation of a quasiequilibrium beam distribution matched to a quadrupole lattice for a broad range of beam intensities and vacuum phase advances describing the strength of the oscillating focusing field. For the case of sufficiently large values of the vacuum phase advance, the deviations of the beam distribution function from the initial state can be significant. Therefore, in the present work, we use the full particle-in-cell code WARP (Ref. 10) to perform the numerical simulations. However, we note that the formalism developed here will also provide a useful approach for initializing the choice of self-consistent quasiequilibrium distributions f_0 in nonlinear δF simulations for intense beam propagation in periodic-focusing lattices.¹¹⁻¹³ Properties of the quasiequilibrium matched beam distribution are investigated in the present analysis. In particular, self-similar evolution of the transverse beam density profile is observed. Furthermore, the density profile of the beam distribution matched to the quadrupole lattice is found to be self-similar to the initial density profile corresponding to the smooth-focusing equilibrium distribution. These observations are consistent with predictions of the Hamiltonian averaging theory developed by Davidson *et al.*⁶ The range of validity of the self-similarity feature is also investigated.

It should be noted that a mismatch between the beam and the transport lattice can produce halo particles, which may cause degradation of the beam quality and activation of the chamber wall.^{14–20} For intense beam accelerators and transport systems it is increasingly important to suppress beam halo production; therefore, quiescent beam matching from the source region into the transport lattice is of particular practical importance.^{21,22} Note that the method developed in this paper for adiabatic formation of a matched beam distribution may possibly be utilized in the design of next-generation transport systems. Indeed, an intense beam produced by an emitting source typically has an azimuthally symmetric envelope with a negligible convergence (divergence) angle and can be easily matched to a uniform focusing channel. Then, a matching section where the oscillating quadrupole field is turned on adiabatically can be used to provide quiescent beam matching to the transport lattice. Conditions on the length of the matching section required to assure that matching is maintained are discussed.

This paper is organized as follows. The theoretical model and assumptions in the present analysis are described in Sec. II. In Sec. III, the approach for the quiescent formation of a quasiequilibrium beam distribution matched to a quadrupole lattice by means of adiabatic turn-on of the oscillating focusing field is investigated for a wide range of transport system parameters, making use of particle-in-cell simulations. Finally, in Sec. IV, properties of the quasiequilibrium matched-beam distribution are investigated and compared with the predictions of the analytical theory developed by Davidson *et al.*⁶

II. THEORETICAL MODEL AND ASSUMPTIONS

In this section, following the analysis in Ref. 9, we summarize the general theoretical model describing the nonlinear dynamics of the beam propagating through an alternating-gradient quadrupole focusing lattice, and the assumptions for the smooth-focusing approximation, which describes the average effects of an alternating-gradient focusing lattice. Here, we consider an axially continuous intense charged particle beam propagating in the z -direction with average axial velocity V_b through a periodic focusing lattice with axial periodicity length $S = \text{const}$. The beam is assumed to be *thin*, with characteristic transverse dimensions a and b in the x and y directions satisfying $a, b \ll S$. Furthermore, it is assumed that the beam self-field perveance, K_b , satisfies

$$K_b \equiv \frac{2N_b e_b^2}{\gamma_b^3 m_b \beta_b^2 c^2} \ll 1,$$

where $N_b = \int dx dy dx' dy' f_b(x, y, x', y', s)$ is the number of particles per unit axial length, $\beta_b = V_b/c$, $\gamma_b = (1 - \beta_b^2)^{-1/2}$ is the relativistic mass factor, e_b and m_b are the charge and rest mass of the beam particles, respectively, and c is the speed of light *in vacuo*. The beam dynamics in the transverse phase space (x, y, x', y') is described by the distribution function $f_b(x, y, x', y', s)$, where $s = s_0 + \beta_b c t$ is the effective axial coordinate, and $x' = dx/ds$ and $y' = dy/ds$ denote the dimensionless transverse velocities. The applied focusing force acting on a beam particle is assumed to be of the form

$$F_{\text{foc}}^q = -\kappa_q(s)[x\hat{\mathbf{e}}_x - y\hat{\mathbf{e}}_y], \quad (1)$$

where $\kappa_q(s) = \kappa_q(s+S)$, and $\int_{s_0}^{s_0+S} ds \kappa_q(s) = 0$. It is readily shown that the nonlinear Vlasov equation describing the evolution of the beam distribution function, f_b , is given by⁹

$$\begin{aligned} \frac{\partial f_b}{\partial s} + x' \frac{\partial f_b}{\partial x} + y' \frac{\partial f_b}{\partial y} - \left[\frac{\partial \psi}{\partial x} + \kappa_q(s)x \right] \frac{\partial f_b}{\partial x'} \\ - \left[\frac{\partial \psi}{\partial y} - \kappa_q(s)y \right] \frac{\partial f_b}{\partial y'} = 0. \end{aligned} \quad (2)$$

Here, the normalized self-field potential $\psi(x, y, s) = e_b \phi(x, y, s) / \gamma_b^3 m_b \beta_b^2 c^2$ is determined self-consistently from

$$\left(\frac{\partial^2}{\partial x^2} + \frac{\partial^2}{\partial y^2} \right) \psi = - \frac{2\pi K_b}{N_b} \int dx' dy' f_b, \quad (3)$$

and $\phi(x, y, s)$ is the beam space-charge potential. Assuming that a perfectly conducting cylindrical wall is located at radius $r = (x^2 + y^2)^{1/2} = r_w$, Eq. (3) is to be solved subject to the boundary condition

$$\left[\frac{1}{r} \frac{\partial \psi(r, \theta)}{\partial \theta} \right]_{r=r_w} = 0, \quad (4)$$

where (r, θ) corresponds to the cylindrical polar coordinates defined by $x = r \cos \theta$ and $y = r \sin \theta$.

Solutions to Eqs. (2)–(4) describe the self-consistent nonlinear evolution of an intense beam propagating through an alternating-gradient quadrupole lattice. Of particular practical importance are the “quasiequilibrium” (matched) solutions in which the beam distribution function is periodic with axial periodicity length equal to the lattice period, i.e., $f_b(x, y, x', y', s+S) = f_b(x, y, x', y', s)$. However, the oscillating nature of the focusing field offers a significant challenge for detailed determination of matched quasiequilibrium solutions. The problem can be significantly simplified if the so-called smooth-focusing approximation,^{1,6,7,9} which describes the average effects of the oscillating focusing field, is used for analysis of the average dynamics of the beam particles. Within this approximation, the average external focusing force has the form

$$F_{\text{foc}}^{sf} = -\kappa_{sf}(x\hat{\mathbf{e}}_x + y\hat{\mathbf{e}}_y), \quad (5)$$

where κ_{sf} is defined by^{1,9}

$$\kappa_{sf} = \left\langle \left(\int_{s_0}^s ds \kappa_q(s) - \left\langle \int_{s_0}^s ds \kappa_q(s) \right\rangle_s \right)^2 \right\rangle_s, \quad (6)$$

and $\langle \dots \rangle_s = S^{-1} \int_{s_0}^{s_0+S} ds \dots$ denotes the average of an s -dependent function over one lattice period S .

In the following analysis we consider a so-called focusing-off defocusing-off transport lattice, in which $\kappa_q(s)$ has the form of a step-function lattice with constant amplitude $\hat{\kappa}_q$ and filling factor η , as shown in Fig. 1. Making use of Eq. (6) it follows that¹

$$\kappa_{sf} = \frac{1}{16} \eta^2 \hat{\kappa}_q^2 S^2 \left(1 - \frac{2}{3} \eta \right). \quad (7)$$

As evident from Eq. (5), within the smooth-focusing approximation, the beam particles exhibit oscillatory motion with axial periodicity length (smooth-focusing period) given

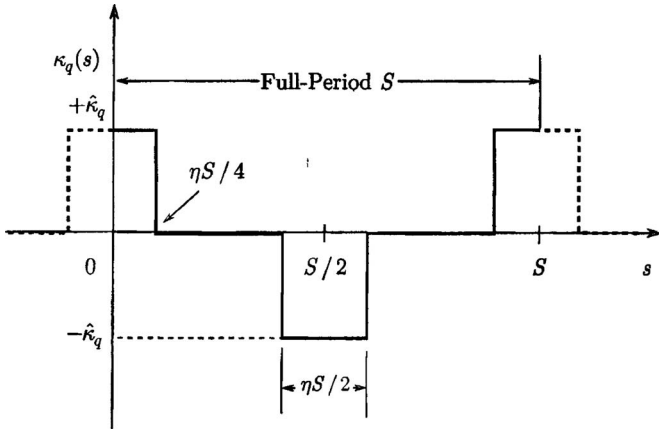


FIG. 1. Alternating-gradient step-function model of a periodic quadrupole lattice with filling factor η for the lens elements. The figure shows a plot of the quadrupole coupling coefficient $\kappa_q(s)$ vs s for one full period (s) of the lattice (see Fig. 3.7 of Ref. 1).

by $2\pi/\sqrt{\kappa_{sf}}$ in the absence of the self-fields. Therefore, it is intuitively appealing to assume that the smooth-focusing approximation is valid if the lattice period is sufficiently small compared to the smooth-focusing period, i.e.,

$$\sqrt{\kappa_{sf}}S/2\pi < 1. \tag{8}$$

It is convenient to introduce dimensionless parameters describing the lattice strength and the beam intensity. For this purpose we introduce the envelope equations that describe (approximately) the evolution of the characteristic transverse beam dimensions $\bar{a}(s)=2\langle x^2 \rangle^{1/2}$ and $\bar{b}(s)=2\langle y^2 \rangle^{1/2}$ (Ref. 1),

$$\frac{d^2}{ds^2}\bar{a} + \left[\kappa_q(s) - \frac{2K_b}{\bar{a}(\bar{a} + \bar{b})} \right] \bar{a} = \frac{\varepsilon^2}{\bar{a}^3}, \tag{9}$$

$$\frac{d^2}{ds^2}\bar{b} + \left[-\kappa_q(s) - \frac{2K_b}{\bar{a}(\bar{a} + \bar{b})} \right] \bar{b} = \frac{\varepsilon^2}{\bar{b}^3}, \tag{10}$$

where we assumed $\varepsilon_x = \varepsilon_y = \varepsilon$, where the transverse emittance, ε_x , is defined by

$$\varepsilon_x = 4\sqrt{\langle(x - \langle x \rangle)^2 \rangle \langle(x' - \langle x' \rangle)^2 \rangle - \langle(x - \langle x \rangle)(x' - \langle x' \rangle)\rangle^2}. \tag{11}$$

Here, $\langle \chi \rangle = N_b^{-1} \int dx dy dx' dy' \chi f_b$ denotes the statistical average of a phase function χ over the beam distribution function, f_b . Note that for the special case of a Kapchinskij-Vladimirskij distribution,^{1,2} the beam density is uniformly distributed within the elliptical cross section $0 \leq [x^2/\bar{a}^2(s) + y^2/\bar{b}^2(s)] \leq 1$, the transverse beam emittance is conserved, $\varepsilon(s) = \text{const}$, and Eqs. (9) and (10) describe the exact evolution of the outer edge (\bar{a}, \bar{b}) of the beam envelope. The average strength of the applied focusing lattice can be described by the vacuum phase advance, σ_v ,

$$\sigma_v \equiv \lim_{K_b \rightarrow 0} \varepsilon \int_{s_0}^{s_0+S} \frac{ds}{\bar{a}^2(s)} = \lim_{K_b \rightarrow 0} \varepsilon \int_{s_0}^{s_0+S} \frac{ds}{\bar{b}^2(s)}, \tag{12}$$

and the effective beam intensity (space-charge strength) can be measured by σ/σ_v , where the depressed phase advance, σ , is defined by

$$\sigma \equiv \varepsilon \int_{s_0}^{s_0+S} \frac{ds}{\bar{a}^2(s)} = \varepsilon \int_{s_0}^{s_0+S} \frac{ds}{\bar{b}^2(s)}. \tag{13}$$

Note that envelope functions $\bar{a}(s)$ and $\bar{b}(s)$ in Eqs. (12) and (13) are the matched solutions to Eqs. (9) and (10) satisfying $\bar{a}(s+S) = \bar{a}(s)$ and $\bar{b}(s+S) = \bar{b}(s)$.

Within the smooth-focusing approximation, the evolution of the characteristic transverse beam dimensions is described (approximately) by the envelope equations (9) and (10) where the terms describing the oscillating force of a quadrupole lattice, i.e., $\kappa_q(s)$ in Eq. (9) and $-\kappa_q(s)$ in Eq. (10), are replaced with the term κ_{sf} corresponding to the smooth-focusing lattice coefficient. The matched smooth-focusing solutions are given by $\bar{a}(s) = \bar{b}(s) = \text{const}$, and it is straightforward to show that in the smooth-focusing approximation the phase advances are determined by¹

$$\sigma_v^{sf} = \sqrt{\kappa_{sf}}S \tag{14}$$

and

$$\frac{\sigma^{sf}}{\sigma_v^{sf}} = \left[1 + \left(\frac{K_b}{2\varepsilon\sqrt{\kappa_{sf}}} \right)^2 \right]^{1/2} - \left(\frac{K_b}{2\varepsilon\sqrt{\kappa_{sf}}} \right). \tag{15}$$

In addition, we note that the normalized beam intensity can be conveniently measured by the following parameter:

$$s_b = \frac{\hat{\omega}_{pb}^2}{2\gamma_b^2\omega_{\beta\perp}^2}, \tag{16}$$

where $\hat{\omega}_{pb} \equiv (4\pi\hat{n}_b e_b^2 / \gamma_b m_b)^{1/2}$ is the relativistic plasma frequency, \hat{n}_b is the on-axis plasma number density, and $\omega_{\beta\perp} \equiv (\kappa_{sf}\beta_b^2 c^2)^{1/2}$ is the average transverse focusing frequency associated with the (smooth-focusing) lattice coefficient κ_{sf} .

III. QUIESCENT LOADING OF A BEAM DISTRIBUTION INTO AN ALTERNATING-GRADIENT QUADRUPOLE LATTICE

In this section we describe the numerical scheme that allows for the quiescent formation of a quasiequilibrium beam distribution matched to an alternating-gradient quadrupole lattice. The scheme is then examined for a range of values of beam intensity and lattice vacuum phase advance, making use of particle-in-cell numerical simulations performed with the 2D slice version of the WARP code. The scheme works as follows. First, the oscillating focusing field of the quadrupole lattice is replaced with the smooth-focusing force given by Eqs. (5) and (7), and the thermal equilibrium beam distribution,

$$f_b^0(H_\perp^0) = \hat{n}_b \left(\frac{\gamma_b m_b \beta_b^2 c^2}{2\pi \hat{T}_{\perp b}} \right) \exp \left\{ - \frac{\gamma_b m_b \beta_b^2 c^2}{\hat{T}_{\perp b}} H_\perp^0 \right\}, \quad (17)$$

is loaded into the uniform channel. Here, the transverse smooth-focusing Hamiltonian, H_\perp^0 , is defined by⁹

$$H_\perp^0 = \frac{1}{2}(x'^2 + y'^2) + \frac{1}{2}\kappa_{sf}r^2 + \psi(r), \quad (18)$$

and $\hat{T}_{\perp b}$ is a positive constant with units of energy. Assuming, without loss of generality, $\psi(r=0)=0$, it readily follows from Eqs. (17) and (18) that \hat{n}_b is the on-axis number density. Then, the oscillating quadrupole focusing force in Eq. (1) is adiabatically turned on, and the uniform focusing component is correspondingly adjusted to maintain the smooth-focusing effect of the total focusing field fixed. That is, the total focusing force acting on the beam particles is specified by

$$F_{\text{foc}}(s) = [V^2(s) - 1]\kappa_{sf}(x\hat{e}_x + y\hat{e}_y) - V(s)\kappa_q(s)(x\hat{e}_x - y\hat{e}_y), \quad (19)$$

where κ_{sf} is defined in Eq. (7), and $V(s)$ is a function describing the smooth transition of the focusing field in the matching section that satisfies $V(s=0)=0$ and $V(s=\infty)=1$. Here, we adopt a simple model in which $V(s)$ varies according to

$$V(s) = \left[1 + \exp\left(\frac{L_{1/2} - s}{L_{tr}}\right) \right]^{-1} - \left[1 + \exp\left(\frac{L_{1/2}}{L_{tr}}\right) \right]^{-1}, \quad (20)$$

where $2L_{1/2}$ is the length of the matching section, and L_{tr} is the characteristic length scale for variation of $V(s)$ from zero to unity provided $L_{1/2} \gg L_{tr}$.

Results of the numerical simulations for the illustrative parameters corresponding to the cases of a space-charge-dominated beam with $2K_b R_{b0}^2 / \varepsilon^2 = 15.3$ ($\sigma / \sigma_v \approx 0.26$), and an emittance-dominated beam with $2K_b R_{b0}^2 / \varepsilon^2 = 0.2$ ($\sigma / \sigma_v \approx 0.91$), are shown in Figs. 2–7. Here, $R_{b0}^2 \equiv \langle (x^2 + y^2) \rangle_0$ is the mean-square beam radius, where $\langle \chi \rangle_0 = N_b^{-1} \int dx dy dx' dy' \chi f_b^0$ denotes the statistical average of a phase function χ over the initial smooth-focusing beam distribution function f_b^0 in Eq. (17). For each value of the beam intensity, the following values of the lattice vacuum phase advance have been considered: $\sigma_v = 44.8^\circ$, $\sigma_v = 65.9^\circ$, and $\sigma_v = 87.5^\circ$. The corresponding values of the phase advances (σ_v^{sf} , σ^{sf}), and normalized beam intensity s_b , calculated for the initial beam equilibrium in the smooth-focusing channel, are indicated in the captions of Figs. 2–7. Other important parameters of the numerical simulations correspond to filling factor $\eta = 0.3$ and wall radius $r_w = 4R_{b0}$; the total number of macroparticles used in the simulation is $N_{pt} = 4 \times 10^6$, and the total number of grid cells in the x and y directions is $N_x = N_y = 128$. To assure that matching is approximately maintained in the matching section, we choose $L_{1/2}/L_{tr} = 5$ and take $L_{1/2} = 5\bar{L}_{sf}$, where \bar{L}_{sf} is the smooth-focusing period of the linear mismatched oscillations determined by¹

$$\bar{L}_{sf} = \frac{2\pi S}{\sqrt{2(\sigma_v^{sf})^2 + 2(\sigma^{sf})^2}}. \quad (21)$$

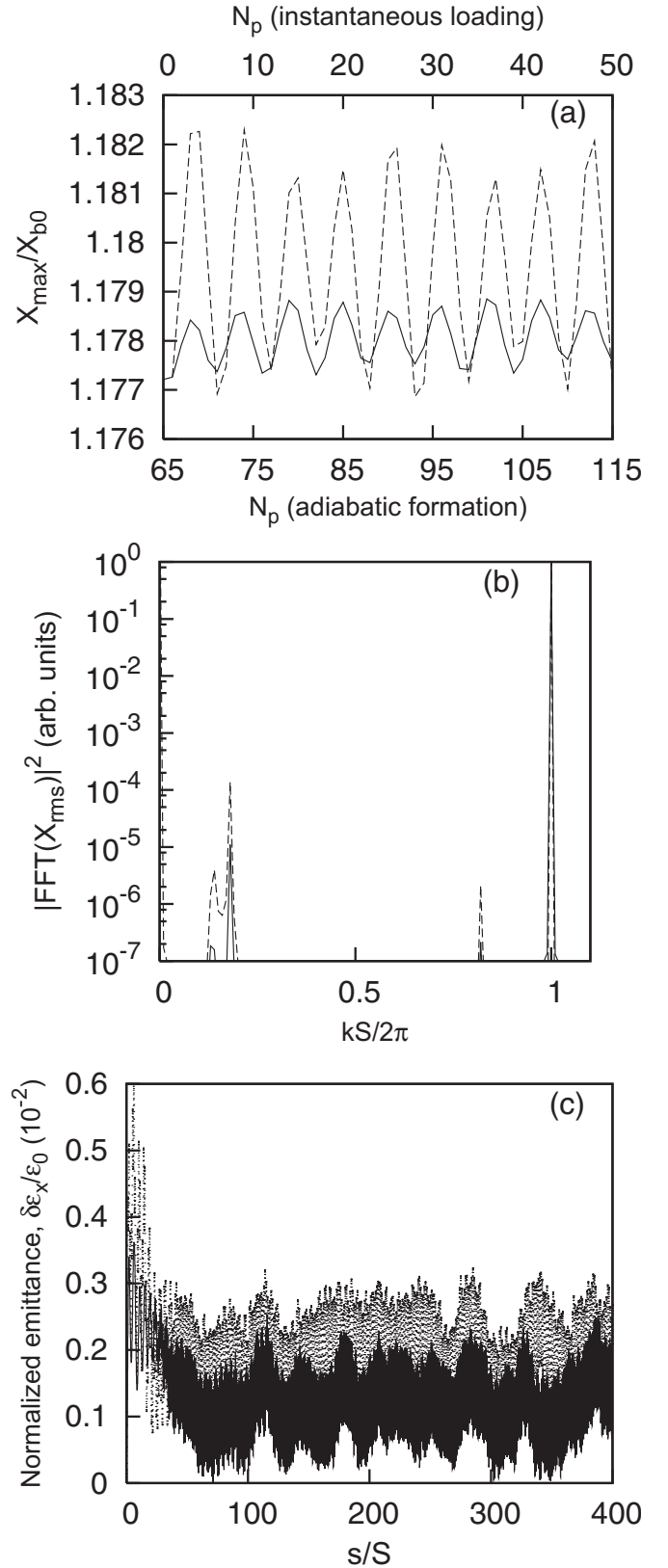


FIG. 2. Evolution of a space-charge-dominated beam with $2K_b R_{b0}^2 / \varepsilon^2 = 15.3$. Phase advances are given by $\sigma_v = 44.8^\circ$ and $\sigma / \sigma_v = 0.255$. The corresponding smooth-focusing parameters are $\sigma_v^{sf} = 43.3^\circ$, $\sigma^{sf} / \sigma_v^{sf} = 0.247$, $s_b = 0.9999$, and $2L_{1/2}/S = 57.1$. The figures show plots of (a) X_{\max}/X_{b0} vs number of lattice periods, N_p , where $X_{b0} = \langle x^2 \rangle_0^{1/2}$, and X_{\max} corresponds to the value of X_{rms} calculated at the end of the focusing cell, (b) FFT of $X_{\text{rms}}(s)$ vs $kS/2\pi$, and (c) normalized perturbed emittance $\delta\varepsilon_x(s)/\varepsilon_0$ vs s/S . The solid curves correspond to an adiabatic turn-on of the lattice, and the dashed curves correspond to the case of an instantaneous beam loading.

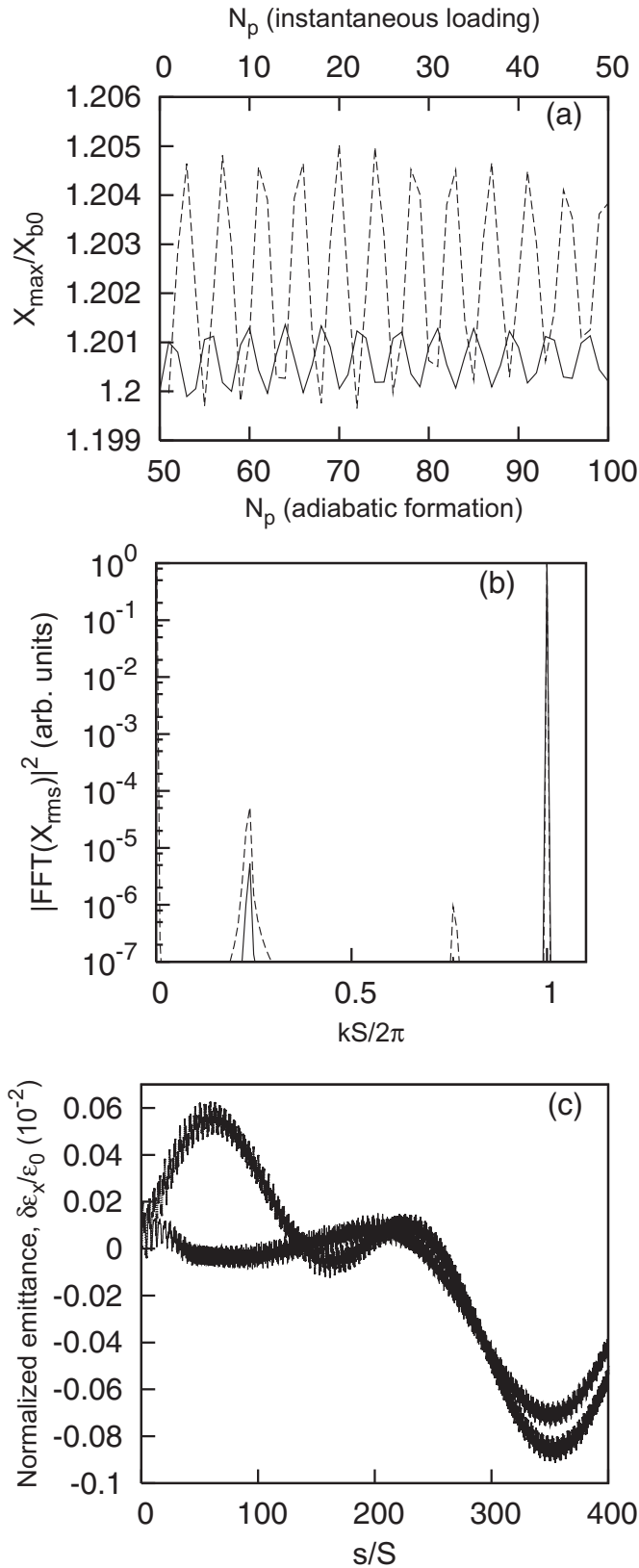


FIG. 3. Evolution of an emittance-dominated beam with $2K_b R_{b0}^2/\epsilon^2=0.2$. Phase advances are given by $\sigma_v=44.8^\circ$ and $\sigma/\sigma_v=0.913$. The corresponding smooth-focusing parameters are $\sigma_v^f=43.3^\circ$, $\sigma^f/\sigma_v^f=0.91$, $s_b=0.32$, and $2L_{1/2}/S=43.5$. The figures show plots of: (a) X_{\max}/X_{b0} vs number of lattice periods, N_p , where $X_{b0}=\langle x^2 \rangle_0^{1/2}$, and X_{\max} corresponds to the value of X_{rms} calculated at the end of the focusing cell, (b) FFT of $X_{\text{rms}}(s)$ vs $kS/2\pi$, and (c) normalized perturbed emittance $\delta\epsilon_x(s)/\epsilon_0$ vs s/S . The solid curves correspond to an adiabatic turn-on of the lattice, and the dashed curves correspond to the case of an instantaneous beam loading.

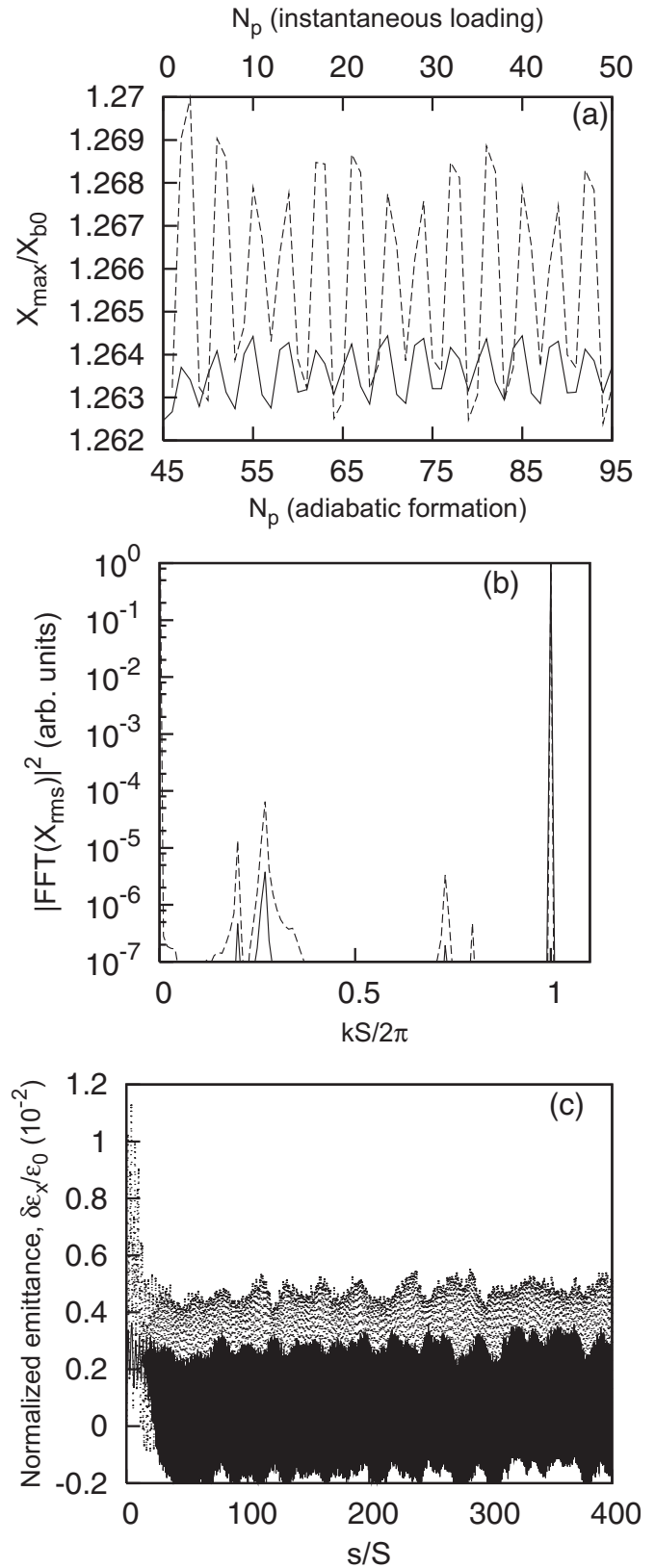


FIG. 4. Evolution of a space-charge-dominated beam with $2K_b R_{b0}^2/\epsilon^2=15.3$. Phase advances are given by $\sigma_v=65.9^\circ$ and $\sigma/\sigma_v=0.260$. The corresponding smooth-focusing parameters are $\sigma_v^f=61.8^\circ$, $\sigma^f/\sigma_v^f=0.247$, $s_b=0.9999$, and $2L_{1/2}/S=40$. The figures show plots of (a) X_{\max}/X_{b0} vs number of lattice periods, N_p , where $X_{b0}=\langle x^2 \rangle_0^{1/2}$ and X_{\max} corresponds to the value of X_{rms} calculated at the end of the focusing cell, (b) FFT of $X_{\text{rms}}(s)$ vs $kS/2\pi$, and (c) normalized perturbed emittance $\delta\epsilon_x(s)/\epsilon_0$ vs s/S . The solid curves correspond to an adiabatic turn-on of the lattice, and the dashed curves correspond to the case of an instantaneous beam loading.

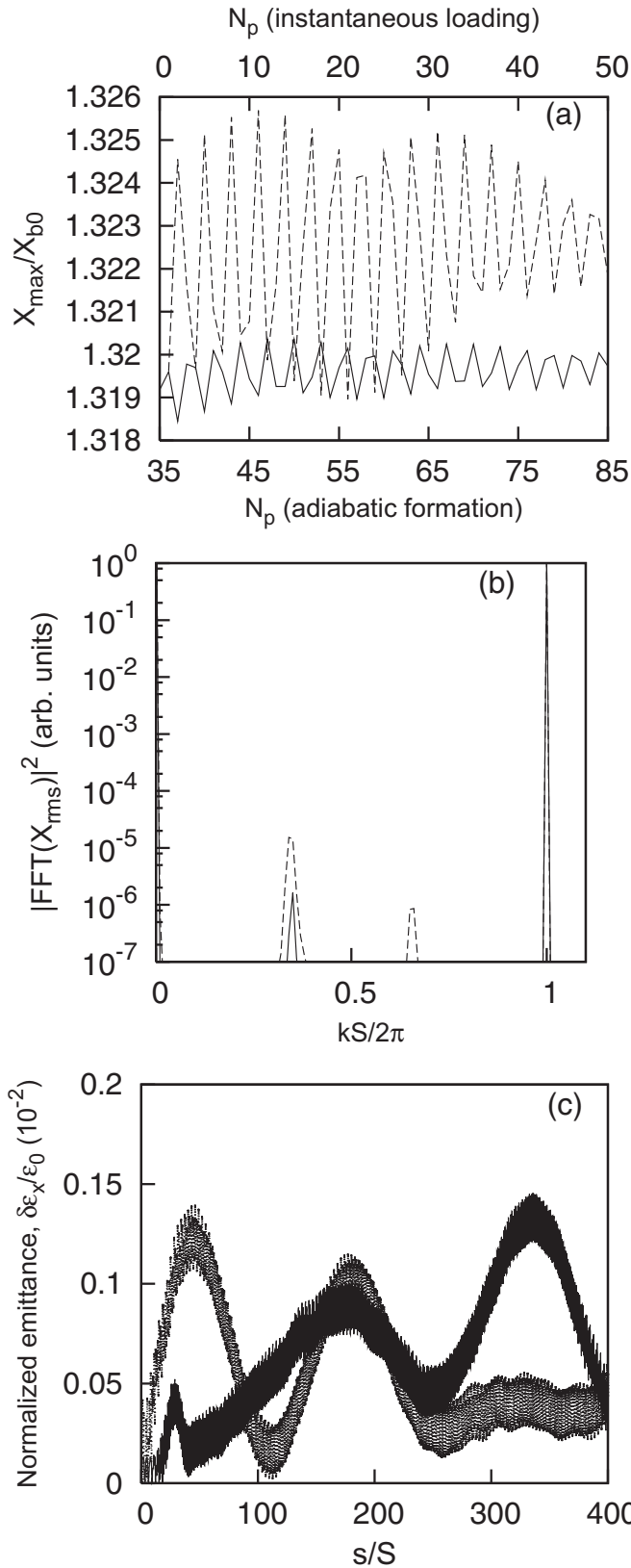


FIG. 5. Evolution of an emittance-dominated beam with $2K_b R_{b0}^2/\epsilon^2=0.2$. Phase advances are given by $\sigma_v=65.9^\circ$ and $\sigma/\sigma_v=0.915$. The corresponding smooth-focusing parameters are $\sigma_v^f=61.8^\circ$, $\sigma^f/\sigma_v^f=0.91$, $s_b=0.32$, and $2L_{1/2}/S=30.5$. The figures show plots of (a) X_{\max}/X_{b0} vs number of lattice periods, N_p , where $X_{b0}=\langle x^2 \rangle_0^{1/2}$, and X_{\max} corresponds to the value of X_{rms} calculated at the end of the focusing cell, (b) FFT of $X_{\text{rms}}(s)$ vs $kS/2\pi$, and (c) normalized perturbed emittance $\delta\epsilon_x(s)/\epsilon_0$ vs s/S . The solid curves correspond to an adiabatic turn-on of the lattice, and the dashed curves correspond to the case of an instantaneous beam loading.

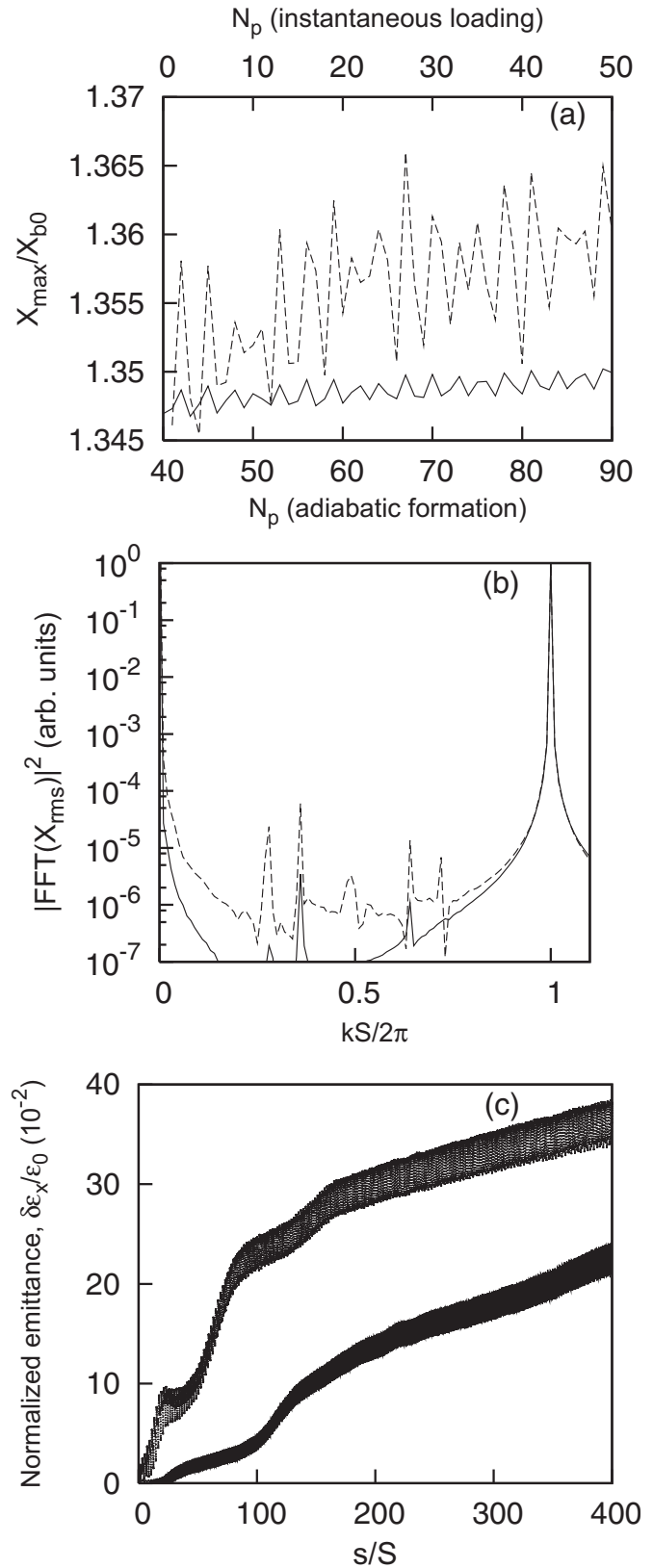


FIG. 6. Evolution of a space-charge-dominated beam with $2K_b R_{b0}^2/\epsilon^2=15.3$. Phase advances are given by $\sigma_v=87.5^\circ$ and $\sigma/\sigma_v=0.265$. The corresponding smooth-focusing parameters are $\sigma_v^f=78.7^\circ$, $\sigma^f/\sigma_v^f=0.247$, $s_b=0.9999$, and $2L_{1/2}/S=31.4$. The figures show plots of (a) X_{\max}/X_{b0} vs number of lattice periods, N_p , where $X_{b0}=\langle x^2 \rangle_0^{1/2}$, and X_{\max} corresponds to the value of X_{rms} calculated at the end of the focusing cell, (b) FFT of $X_{\text{rms}}(s)$ vs $kS/2\pi$, and (c) normalized perturbed emittance $\delta\epsilon_x(s)/\epsilon_0$ vs s/S . The solid curves correspond to an adiabatic turn-on of the lattice, and the dashed curves correspond to the case of an instantaneous beam loading.

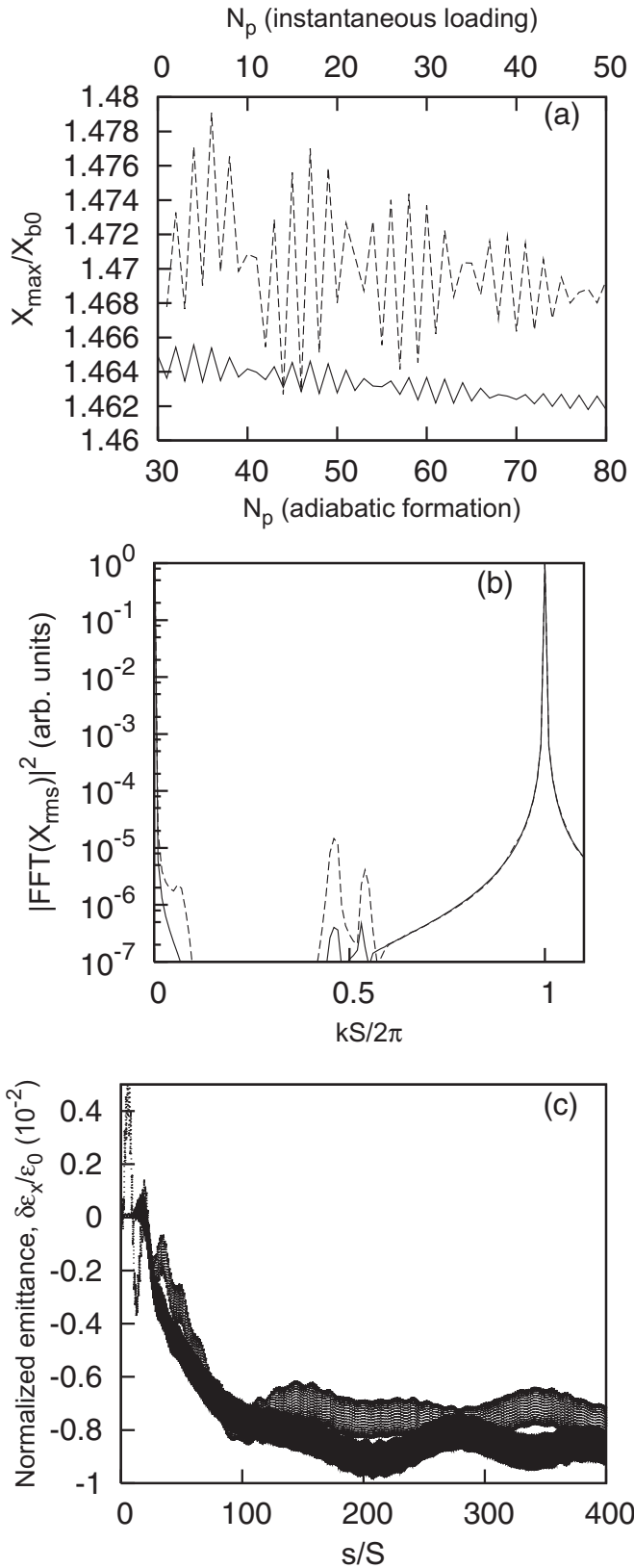


FIG. 7. Evolution of an emittance-dominated beam with $2K_b R_{b0}^2/\epsilon^2=0.2$. Phase advances are given by $\sigma_v=87.5^\circ$ and $\sigma/\sigma_v=0.918$. The corresponding smooth-focusing parameters are $\sigma_v^f=78.7^\circ$, $\sigma^f/\sigma_v^f=0.91$, $s_b=0.32$, and $2L_{1/2}/S=23.9$. The figures show plots of (a) X_{\max}/X_{b0} vs number of lattice periods, N_p , where $X_{b0}=\langle x^2 \rangle_0^{1/2}$, and X_{\max} corresponds to the value of X_{rms} calculated at the end of the focusing cell, (b) FFT of $X_{\text{rms}}(s)$ vs $kS/2\pi$, and (c) normalized perturbed emittance $\delta\epsilon_x(s)/\epsilon_0$ vs s/S . The solid curves correspond to an adiabatic turn-on of the lattice, and the dashed curves correspond to the case of an instantaneous beam loading.

In each of Figs. 2–7, the frames in (a) illustrate the discrete evolution of the normalized rms envelope x -dimension, $X_{\text{rms}} \equiv \langle x^2 \rangle^{1/2}$, calculated at the end of each focusing cell where the beam x -envelope has a local maximum value. Such a graphical representation for a matched beam would be a horizontal straight line; therefore (a) provides a convenient representation of beam mismatch. The frames in (b) show fast-Fourier transform (FFT) plots of $X_{\text{rms}}(s)$, where the continuous evolution of $X_{\text{rms}}(s)$ is used for the FFT calculations. Finally, the frames in (c) show the evolution of the x -component of the normalized perturbations in transverse beam emittance, $\delta\epsilon_x(s)/\epsilon_0 \equiv [\epsilon_x(s) - \epsilon_x(s=0)]/\epsilon_x(s=0)$. Along with the evolution of the beam parameters for the case of adiabatic turn-on of $V(s)$ shown by the solid curves, Figs. 2–7 also show the evolution of beam parameters (dashed curves) for the case where the initial distribution is loaded instantaneously into an alternating-gradient quadrupole lattice with $V(s) \equiv 1$.²³ To load particles for this case, first the matched solutions to the envelope equations (9) and (10) are found. Then, the smooth-focusing thermal equilibrium distribution that satisfies $2R_{b0}^2 = \bar{a}^2(s') = \bar{b}^2(s')$ is calculated. Here s' denotes the location inside the focusing cell where $\bar{a}(s') = \bar{b}(s')$. Finally, the positions and velocities of the beam particles are linearly scaled providing the size and the slope of the beam envelope to be consistent with the matched solution to the envelope equations (9) and (10). Note that the frames in (a) in Figs. 2–7 illustrate the initial evolution of the beam mismatch for the case of instantaneous loading, and the evolution near the exit of the matching section, $s > 2L_{1/2}$, for the case of the adiabatic formation of a beam quasiequilibrium. Correspondingly, the averages for the FFT calculations are from $s=0$ to $s=100S$ for the case of instantaneous loading, and from $s=2L_{1/2}$ to $s=2L_{1/2}+100S$ for the case of adiabatic turn-on of $V(s)$. Note that the 100-lattice-period window for the FFT averages is found to be sufficient for present purposes. It allows us to resolve the difference between the even (symmetric) and the odd (quadrupole) mismatch envelope mode frequencies as seen in Figs. 2, 4, and 6. Furthermore, for the case of an emittance-dominated beam the mismatch oscillations are significantly damped after ~ 100 lattice periods; therefore an increase in the FFT-average window would result in noise integration.

It is evident from Figs. 2–7, for the case of adiabatic formation of the beam quasiequilibrium, that the amplitude of the mismatch oscillations is reduced compared to the case of instantaneous loading of the distribution. Furthermore, note that for the case of adiabatic formation the beam mismatch is attributed primarily to the numerical imprecision in loading the initial smooth-focusing equilibrium distribution, and therefore can be further suppressed if a finer grid structure, and larger number of macroparticles are used in the simulations. In contrast, the numerical scheme for instantaneous loading cannot provide the detailed quasiequilibrium intrinsically. Note that mismatch relaxation is more pronounced for the case of an emittance-dominated beam compared to the case of a space-charge-dominated beam, which is consistent with the studies in Refs. 17, 18, and 24. Of particular interest is the case of intense beam propagation

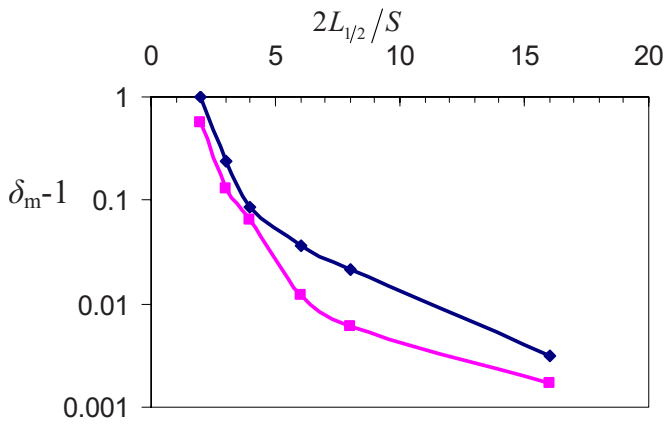


FIG. 8. (Color online) Degree of beam mismatch at the end of the matching section plotted vs the length of the matching section. Here, the vacuum phase advance is $\sigma_v=65.9^\circ$, and the two cases correspond to normalized intensity $2K_b R_{b0}^2/\epsilon^2=15.3$ (blue diamonds) and $2K_b R_{b0}^2/\epsilon^2=0.2$ (pink squares).

($2K_b R_{b0}^2/\epsilon^2=15.3$) through the quadrupole lattice with moderately high vacuum phase advance ($\sigma_v=87.5^\circ$). In this case, appreciable emittance growth is evident even for adiabatic formation of the beam distribution [Fig. 6(c)]. The simulations demonstrate that the beam is well-matched to the lattice for over 450 lattice periods, and therefore the increase in the beam emittance cannot be attributed to mismatch relaxation. A plausible explanation of this phenomena can be attributed to “higher-order resonance” effects, which limit intense beam transport in the region where $\sigma_{vac}^2 - \sigma^2 > (2\pi/3)^2/2$,^{25,26} as proposed in Ref. 27. As the system parameters approach this stability limit, higher-order resonances appear near the beam core in the transverse phase-space; therefore, near-edge particles can diffuse outside the beam core sufficiently to partake in the resonances, thus providing emittance growth.²⁷

The matching section that provides adiabatic lattice transition from a uniform channel to an alternating-gradient quadrupole lattice could in principle be utilized to provide beam matching from the source into the quadrupole lattice for next-generation accelerators and transport systems. It is therefore of particular practical importance to estimate how smooth (adiabatic) the lattice transition should be to assure that matching is maintained during the transition. Figure 8

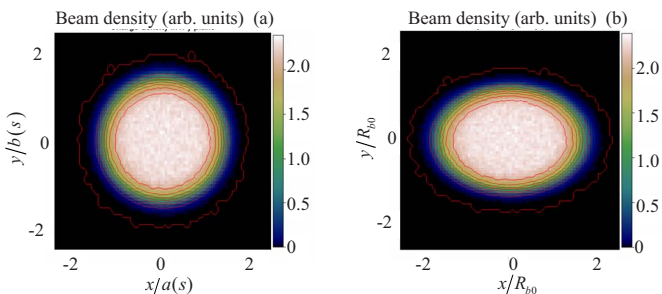


FIG. 9. (Color online) Contour plots of the beam density calculated at the end of the focusing cell and plotted in (a) scaled and (b) regularly normalized coordinates. The vacuum phase advance is $\sigma_v=44.8^\circ$, and the normalized beam intensity corresponds to $2K_b R_{b0}^2/\epsilon^2=15.3$.

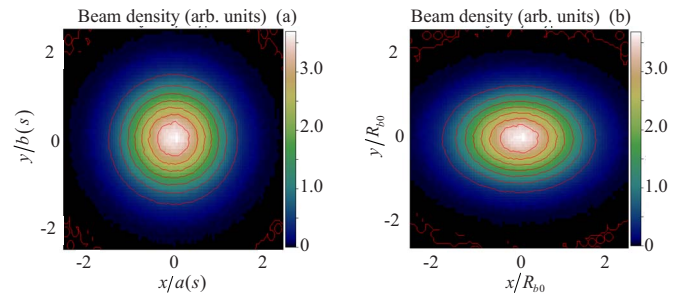


FIG. 10. (Color online) Contour plots of the beam density calculated at the end of the focusing cell and plotted in (a) scaled and (b) regularly normalized coordinates. The vacuum phase advance is $\sigma_v=44.8^\circ$, and the normalized beam intensity corresponds to $2K_b R_{b0}^2/\epsilon^2=0.2$.

illustrates the degree of beam mismatch, δ_m , calculated at the end of the matching section ($s > 2L_{1/2}$) for different values of the matching section length, $2L_{1/2}$, for the case where the vacuum phase advance of the lattice σ_v is 65.9° . Here, we measure the beam mismatch, δ_m , by the ratio of the maximum to minimum values of $X_{rms} \equiv \langle x^2 \rangle^{1/2}$ calculated at the end of each focusing cell within the first two periods of the smooth-focusing mismatch oscillations after the beam leaves the matching section, i.e., within the range $2L_{1/2} < s < 2L_{1/2} + 2\bar{L}_{sf}$. Recall that the beam rms envelope x -dimension, X_{rms} , has a local maximum at the end of a focusing cell. It is readily seen from Fig. 8 that a moderate length of the matching section, approximately ten lattice periods, is sufficient to assure that the beam is well-matched to the lattice. Furthermore, a longer matching section is required for higher beam intensities. It should be noted that these observations are consistent with the results of detailed numerical and experimental studies in Refs. 17, 18, 28, and 29 of the beam response to the smooth variations of the lattice amplitude.

IV. SELF-SIMILAR EVOLUTION OF THE BEAM DENSITY PROFILE

In the previous section we demonstrated that the formation of a quasiequilibrium beam distribution matched to an alternating-gradient quadrupole focusing lattice can be achieved in the numerical simulations by means of the adia-

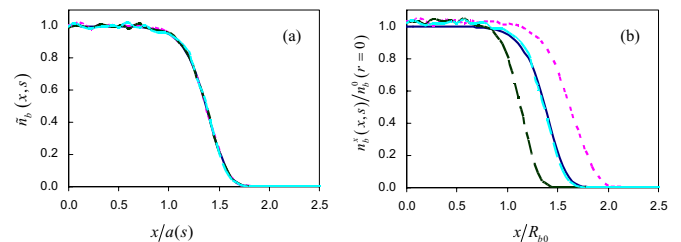


FIG. 11. (Color online) Plots of the beam density profile for a space-charge-dominated beam with $2K_b R_{b0}^2/\epsilon^2=15.3$. Phase advances are given by $\sigma_v=44.8^\circ$ and $\sigma/\sigma_v=0.255$. Shown are (a) normalized density profile, $\bar{n}_b(x,s)=[a(s)b(s)/R_{b0}^2][n_b^s(x,s)/n_b^0(r=0)]$, vs the scaled transverse coordinate $x/a(s)$; and (b) $\bar{n}_b^s(x,s)/n_b^0(r=0)$ vs x/R_{b0} . Density profiles correspond to: the initial smooth-focusing thermal equilibrium (solid blue curve), the maximum value of X_{rms} (dotted pink curve), the minimum value of X_{rms} (dashed green curve), and the location inside the focusing cell where $X_{rms} = Y_{rms}$ (dot-dashed cyan curve).

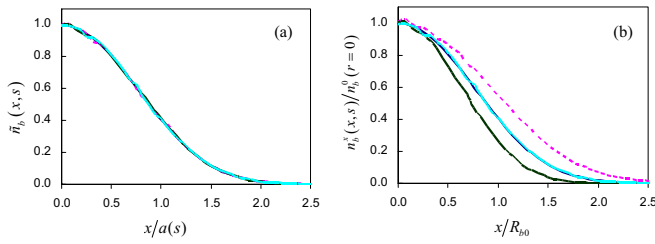


FIG. 12. (Color online) Plots of the beam density profile for an emittance-dominated beam with $2K_b R_{b0}^2/\varepsilon^2=0.2$. Phase advances are given by $\sigma_v=44.8^\circ$ and $\sigma/\sigma_v=0.913$. Shown are (a) normalized density profile, $\tilde{n}_b(x,s)=[a(s)b(s)/R_{b0}^2][n_b^x(x,s)/n_b^0(r=0)]$, vs the scaled transverse coordinate $x/a(s)$, and (b) $n_b^x(x,s)/n_b^0(r=0)$ vs x/R_{b0} . Density profiles correspond to the initial smooth-focusing equilibrium (solid blue curve), the maximum value of X_{rms} (dotted pink curve), the minimum value of X_{rms} (dashed green curve), and the location inside the focusing cell where $X_{rms}=Y_{rms}$ (dot-dashed cyan curve).

batic turn-on of the oscillating focusing field. In this section we investigate properties of the matched beam distribution in order to compare results of the numerical simulations with predictions of the analytical theory developed by Davidson *et al.*⁶ Furthermore, we make use of the numerical simulations to investigate the validity limits of the theory. The analytical model developed in Refs. 1, 6, and 7 applies Hamiltonian averaging techniques to the nonlinear Vlasov–Maxwell equations (2) and (3), assuming sufficiently small vacuum phase advance, σ_v . It has been demonstrated that the evolution of the beam density profile for the case of intense beam propagation through an alternating gradient–quadrupole lattice is given by^{1,6}

$$n_b(x,y,s) = \frac{R_{b0}^2}{a(s)b(s)} n_b^0 \left[\frac{\tilde{R}(x,y,s)}{R_{b0}} \right], \quad (22)$$

correct to order ε^3 , where $\varepsilon \equiv \sigma_v/2\pi$ is the expansion parameter of the theory. Here, $n_b^0(r)$ is the beam density profile corresponding to an arbitrary smooth-focusing equilibrium, and $\tilde{R}(x,y,s)/R_{b0}$ is defined by

$$\frac{\tilde{R}(x,y,s)}{R_{b0}} = \left[\frac{x^2}{a^2(s)} + \frac{y^2}{b^2(s)} \right]^{1/2}, \quad (23)$$

where $a(s)=\sqrt{2}X_{rms}(s)$ and $b(s)=\sqrt{2}Y_{rms}(s)$. Note that the theory assumes that the conducting wall is sufficiently far removed from the beam ($r_w \rightarrow \infty$).

We now investigate properties of the quasiequilibrium beam density profiles obtained in the numerical simulations for the illustrative parameters considered in Sec. III, and compare it with predictions of the analytical theory given by Eqs. (22) and (23). For all of the simulations we take $r_w=4R_{b0}$, which corresponds to a sufficiently large radius of the conducting wall. Results of the numerical simulations are presented in Figs. 9–14, and the density profiles shown in the figures are calculated within the first lattice period after the beam leaves the matching section, i.e., $2L_{1/2} < s < 2L_{1/2} + S$. Figures 9 and 10 show contour plots of the beam density for the cases of a space-charge-dominated beam with $2K_b R_{b0}^2/\varepsilon^2=15.3$ (Fig. 9), and an emittance-dominated beam with $2K_b R_{b0}^2/\varepsilon^2=0.2$ (Fig. 10). It is readily seen from the

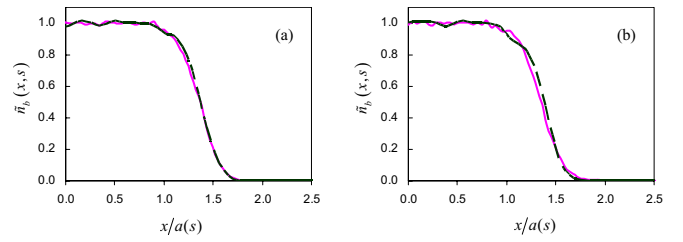


FIG. 13. (Color online) Plots of the normalized beam density profile, $\tilde{n}_b(x,s)=[a(s)b(s)/R_{b0}^2][n_b^x(x,s)/n_b^0(r=0)]$, for a space-charge-dominated beam with $2K_b R_{b0}^2/\varepsilon^2=15.3$. Phase advances are given by (a) $\sigma_v=65.9^\circ$, $\sigma/\sigma_v=0.260$ and (b) $\sigma_v=87.5^\circ$, $\sigma/\sigma_v=0.265$. Density profiles correspond to the maximum value of X_{rms} (solid pink curve) and the minimum value of X_{rms} (dashed green curve).

figures that, plotted in the scaled coordinates $\{x/a(s), y/b(s)\}$, the contours of constant beam density are approximately circular, which is consistent with Eqs. (21) and (22). Therefore, without loss of generality, in the following analysis we present results of the numerical simulations for the evolution of the beam density projected along the x -direction, $n_b^x(x,s) \equiv n_b(x,y=0,s)$. Figures 11 and 12 show the evolution of the beam density plotted in scaled coordinates [Figs. 11(a) and 12(a)] and regularly normalized coordinates [Figs. 11(b) and 12(b)] for the cases where $2K_b R_{b0}^2/\varepsilon^2=15.3$ and $2K_b R_{b0}^2/\varepsilon^2=0.2$, respectively. For these simulations, a relatively modest value of the vacuum phase advance of $\sigma_v=44.8^\circ$ is considered. It is readily seen that the evolution of the quasiequilibrium beam density is self-similar, i.e., $n_b^x(x,s) \approx n_b^x[x/a(s)]$ to very good approximation. Note that the flutter on top of the beam density profiles in Figs. 11 and 12 is due to the numerical noise, and much lower noise level has been observed in the numerical simulations with a larger number of macroparticles ($N_{pt}=6 \times 10^6$) and coarser grid ($N_x=N_y=64$). Furthermore, to good visual accuracy, it is evident that the beam density evolution in the quadrupole lattice is also self-similar to the initial beam density profile (plotted in Figs. 11 and 12 by the blue curves) corresponding to the initial smooth-focusing thermal equilibrium with the distribution function in Eq. (17). Analytical theory^{1,6} predicts that the beam density profile is self-similar to the density profile determined from the choice of smooth-focusing equilibrium distribution function. However, it is interesting to note that the smooth-focusing equilibrium

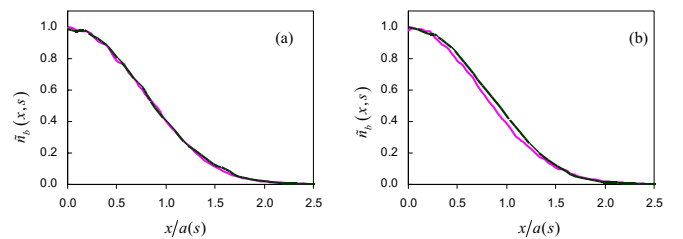


FIG. 14. (Color online) Plots of the normalized beam density profile, $\tilde{n}_b(x,s)=[a(s)b(s)/R_{b0}^2][n_b^x(x,s)/n_b^0(r=0)]$ for an emittance-dominated beam with $2K_b R_{b0}^2/\varepsilon^2=0.2$. Phase advances are given by (a) $\sigma_v=65.9^\circ$, $\sigma/\sigma_v=0.915$ and (b) $\sigma_v=87.5^\circ$, $\sigma/\sigma_v=0.918$. Density profiles correspond to the maximum value of X_{rms} (solid pink curve) and the minimum value of X_{rms} (dashed green curve).

corresponding to the beam distribution matched to the quadrupole lattice remains the same during the adiabatic transition phase in the matching section.

Finally, Figs. 13 and 14 show the beam density evolution plotted in scaled coordinates for larger values of the vacuum phase-advance $\sigma_v=65.9^\circ$ and $\sigma_v=87.5^\circ$. It is readily seen that the beam density evolution is still self-similar to good visual accuracy for $\sigma_v=65.9^\circ$. However, a more pronounced difference in the density profiles in the fall-off region occurs for $\sigma_v=87.5^\circ$ for both space-charge-dominated and emittance-dominated beams. This illustrates the range of validity of the analytical predictions given by Eqs. (21) and (22). Again, we note that the flutter on top of the beam density profiles in Figs. 13 and 14 can be substantially suppressed if a larger number of macroparticles is used in the simulations; however, in the density-fall-off region, the difference in the beam density profiles shown in Figs. 13(b) and 14(b) remains nearly the same. It is particularly interesting to note, for the case of an emittance-dominated beam with $\sigma/\sigma_v=0.918$ and $\sigma_v=87.5^\circ$, that the beam transport is stable, the effects of higher-order resonances are weak, and yet the analytical theory predictions is of limited validity.

V. CONCLUSIONS

In this work we described a numerical scheme allowing for the formation of a quasiequilibrium beam distribution matched to an alternating-gradient quadrupole focusing lattice by means of adiabatic turn-on of the oscillating focusing field. The scheme demonstrates the ability to load a matched-beam distribution into a quadrupole lattice for a broad range of beam intensity and vacuum phase advance $\sigma_v \lesssim 66^\circ$. Furthermore, for higher values of vacuum phase advance (for instance, $\sigma_v=87.5^\circ$), even in a regime where the parameters of the transport system approach the unstable transport criterion given by $\sigma_v^2 - \sigma^2 > (2\pi/3)^2/2$, and the transport of the intense beam is accompanied by beam emittance growth, it is found that the method of adiabatic formation described here still provides adequate beam matching. Therefore, the scheme described here can be effectively used for detailed studies of intense beam transport and stability properties, since it is able to suppress the effects of the initial beam mismatch. Finally, it is found that a moderate length of the matching section (~ 10 lattice periods) is sufficient to assure that the beam is well matched to the lattice, thus making the scheme attractive for practical applications.

Properties of the matched beam quasiequilibrium obtained in the numerical simulations have been investigated and compared with the predictions of the analytical theory developed by Davidson *et al.* in Ref. 6. The theory shows that for sufficiently small values of $\varepsilon \equiv \sigma_v/2\pi$, the evolution of the beam density is self-similar correct to ε^3 . In accordance with the theory, the numerical simulations demonstrate self-similar evolution of the beam density profile for $\sigma_v \lesssim 66^\circ$. However, for higher values of vacuum phase advance (for instance, $\sigma_v=87.5^\circ$) the self-similarity feature becomes less accurate for wide range of beam intensities, which demonstrates the validity limits of the theory.

It should be noted that the formalism developed here can provide a useful approach for initializing the choice of self-consistent quasiequilibrium distributions f_0 in nonlinear δF simulations^{11–13} for intense beam propagation in periodic-focusing lattices. Finally, the present approach can be generalized in straightforward manner to the case of a periodic focusing solenoidal lattice.

ACKNOWLEDGMENTS

The authors are grateful to Steve Lund for the benefit of fruitful discussions.

This research was supported by the U.S. Department of Energy under Contract No. DE-AC02-76CH-O3073 with the Princeton Plasma Physics Laboratory.

¹R. C. Davidson and H. Qin, *Physics of Intense Charged Particle Beams in High Energy Accelerators* (World Scientific, Singapore, 2001) (and references therein).

²M. Reiser, *Theory and Design of Charged Particle Beams* (Wiley, New York, 1994).

³A. W. Chao, *Physics of Collective Beam Instabilities in High Energy Accelerators* (Wiley, New York, 1993).

⁴See, for example, *Proceedings of the Particle Accelerator Conference, Albuquerque, 2007* (IEEE, Piscataway, NJ, 2007).

⁵*Proceedings of the 17th International Symposium on Heavy Ion Inertial Fusion, 2008*, Nucl. Instrum. Methods Phys. Res. A **606** (1–2) (2009).

⁶R. C. Davidson, H. Qin, and P. Channell, *Phys. Rev. ST Accel. Beams* **2**, 074401 (1999); **3**, 029901 (2000).

⁷P. J. Channell, *Phys. Plasmas* **6**, 982 (1999).

⁸P. H. Stoltz, R. C. Davidson, and W. W. Lee, *Phys. Plasmas* **6**, 298 (1999).

⁹R. C. Davidson and H. Qin, *Phys. Rev. ST Accel. Beams* **4**, 104401 (2001).

¹⁰A. Friedman, D. P. Grote, and I. Haber, *Phys. Fluids B* **4**, 2203 (1992).

¹¹H. Qin, R. Davidson, and E. Startsev, *Phys. Rev. ST Accel. Beams* **10**, 064201 (2007).

¹²E. Startsev, R. Davidson, and H. Qin, *Phys. Plasmas* **14**, 056705 (2007).

¹³H. Qin, R. Davidson, and E. Startsev, *Phys. Plasmas* **15**, 063101 (2008).

¹⁴R. L. Gluckstern, *Phys. Rev. Lett.* **73**, 1247 (1994).

¹⁵T. P. Wangler, K. R. Crandall, R. Ryne, and T. S. Wang, *Phys. Rev. ST Accel. Beams* **1**, 084201 (1998).

¹⁶J. Qiang, P. L. Colestock, D. Gilpatrick, H. V. Smith, T. P. Wangler, and M. E. Schulze, *Phys. Rev. ST Accel. Beams* **5**, 124201 (2002).

¹⁷M. Dorf, R. C. Davidson, and E. A. Startsev, *Phys. Rev. ST Accel. Beams* **9**, 034202 (2006).

¹⁸M. Dorf, R. C. Davidson, and E. A. Startsev, *Proceedings of the Particle Accelerator Conference, Albuquerque, 2007* (IEEE, Piscataway, NJ, 2007), p. 3669.

¹⁹R. Gluckstern, A. Fedetov, S. Kurennoy, and R. Ryne, *Phys. Rev. E* **58**, 4977 (1998).

²⁰M. Ikegami, *Phys. Rev. E* **59**, 2330 (1999).

²¹Y. K. Batygin, *Phys. Rev. E* **54**, 5673 (1996).

²²L. R. Prost, P. A. Seidl, F. M. Bieniosek, C. M. Celata, A. Falten, D. Baca, E. Henestroza, J. W. Kwan, M. Leitner, W. L. Waldron, R. Cohen, A. Friedman, D. Grote, S. M. Lund, A. W. Molvik, and E. Morse, *Phys. Rev. ST Accel. Beams* **8**, 020101 (2005).

²³S. Lund, T. Kikuchi, and R. Davidson, *Phys. Rev. ST Accel. Beams* **12**, 114801 (2009).

²⁴V. Variale, *Phys. Rev. ST Accel. Beams* **4**, 084201 (2001).

²⁵M. G. Tiefenback and D. Keffe, *IEEE Trans. Nucl. Sci.* **NS-32**, 2483 (1985).

²⁶M. G. Tiefenback, "Space-charge limits on the transport of ion beams," Ph.D. thesis, U.S. Berkeley, 1986; Lawrence Berkeley Laboratory Report No. LBL-22465, 1986.

²⁷S. M. Lund and S. R. Chawla, *Nucl. Instrum. Methods Phys. Res. A* **561**, 203 (2006).

²⁸M. Chung, E. P. Gilson, M. Dorf, R. C. Davidson, P. C. Efthimion, and R. Majeski, *Phys. Rev. ST Accel. Beams* **10**, 064202 (2007).

²⁹E. P. Gilson, M. Chung, R. C. Davidson, M. Dorf, D. P. Grote, P. C. Efthimion, R. Majeski, and E. A. Startsev, *Nucl. Instrum. Methods Phys. Res. A* **577**, 117 (2007).